Journal of Alloys and Compounds 705 (2017) 492–496

Contents lists available at ScienceDirect

Journal of Alloys and Compounds

journal homepage: http://www.elsevier.com/locate/jalcom

# Giant enhancement of ultraviolet near-band-edge emission from a wide-bandgap oxide with dipole-forbidden bandgap transition

Hang Zhou [a], Rui Deng [a, *], Yongfeng Li [b, c], Bin Yao [b, c, **], Jieming Qin [a], Jing Song [a], Yuqian Li [b], Zhanhui Ding [b, c], Lei Liu [d]

[a] School of Materials Science and Engineering, Changchun University of Science and Technology, Changchun, 130022, China
[b] Key Laboratory of Physics and Technology for Advanced Batteries (Ministry of Education), College of Physics, Jilin University, Changchun, 130012, China
[c] State Key Lab of Superhard Material, and College of Physics, Jilin University, Changchun, 130012, China
[d] State Key Laboratory of Luminescence and Applications, Changchun Institute of Optics, Fine Mechanics and Physics, Chinese Academy of Sciences, No. 3888 Dongnanhu Road, Changchun 130033, China

ARTICLE INFO

*Article history:*
Received 8 January 2017
Received in revised form
10 February 2017
Accepted 11 February 2017
Available online 16 February 2017

*Keywords:*
$SnO_2$
Ag doping
Surface plasmon
Photoluminescence
First-principles calculation

ABSTRACT

We report giant enhancement of recovered ultraviolet near-band-edge emission from $SnO_2$ thin films with dipole-forbidden bandgap transition via Ag-doping and surface plasmon coupling. It is found that a recovering near-band-edge emission in the range of 361–375 nm in a low-concentration Ag-doped $SnO_2$ film, suggesting that dipole-forbidden transition rule of $SnO_2$ is broken. First-principles electronic structure calculations indicate that the breaking of the dipole-forbidden transition rule is derived from the acceptor of Ag substituting Sn in $SnO_2$. 30-fold enhancement of ultraviolet near-band-edge emission from the Ag-doped $SnO_2$ film is observed by modifying film surface using Ag nanoparticles. The giant enhancement of ultraviolet emission is ascribed to surface plasmon coupling between Ag-doped $SnO_2$ and Ag nanoparticles. Our results suggest that Ag doping and Ag nanoparticles surface modification in $SnO_2$ films play important roles in recovering and enhancing ultraviolet emission of $SnO_2$ with dipole-forbidden bandgap transition.



## 1. Introduction

Wide-bandgap oxides have attracted much attention due to their rich functionalities and technological applications [1–11]. Among these oxides, tin dioxide ($SnO_2$), as a wide bandgap semiconductor, has been applied in the fields of transparent conducting thin films, solar cells, gas sensors, catalysis and so on [12–18]. Although bulk $SnO_2$ has a wide direct bandgap of ~3.6 eV, it cannot efficiently emit ultraviolet (UV) light due to the dipole-forbidden nature of its band edge quantum states [19], which has hindered its potential use in optoelectronic applications, such as photodetectors and light-emitting diodes (LEDs). In our previous work, to recover the optical activity of $SnO_2$ and realize the UV near-band-edge (NBE) emission, we utilized nanoengineering and doping engineering to modify $SnO_2$ electronic structure so that the dipole-forbidden rule can be broken and we also demonstrated $SnO_2$-based UV LEDs [12,13]. However, the intensity of UV emission from the $SnO_2$ layer is still weak. Recent decade, Surface plasmons (SPs) have been widely used to improve the emission efficiency of light emitting materials and devices [20]. For instance, Okamoto. *et al* reported the SPs enhanced light emitters based on InGaN quantum wells [21]. To achieve enhancement of UV emission induced by SPs, one of key factors is the energy match. The exciton energy can be rapidly transferred to plasmon excitation when the large frequency overlaps between SPs electric field and semiconductors [22,23]. Therefore, the key to enhance the UV emission is to choose the appropriate metal. Grontijo et al. reported that the first example of resonance coupling of the semiconductor spontaneous emission into SPs [24]. For metal Ag, the bulk plasmon energy is 3.7 eV and the SPs energy is somewhat lower, depending on the retroactive index of the adjacent dielectric [25–27]. The result indicates that this energy range is fortunate since the $SnO_2$ can be resonant with Ag SPs. Hence, the feature of the Ag surface plasmon resonance (SPR) effect can be also applied to the field of $SnO_2$ thin films to enhance the UV emission. To the best of our knowledge,

* Corresponding author.
** Corresponding author. School of Materials Science and Engineering, Changchun University of Science and Technology, Changchun, 130022, China
*E-mail addresses:* dengrui79@126.com (R. Deng), binyao@jlu.edu.cn (B. Yao).

http://dx.doi.org/10.1016/j.jallcom.2017.02.119
0925-8388/

there has been no report on enhancement of the UV emission in $SnO_2$ thin films.

In this paper, we demonstrate the recovering UV emission in the $SnO_2$ thin film with dipole-forbidden bandgap transition via Ag-doping and the UV giant enhancement induced by SPR effect in the Ag-doped $SnO_2$ film with surface modification using Ag nanoparticles ($SnO_2$:Ag/Ag nanoparticles hybrid films).

## 2. Experimental process and first-principles calculations detail

The $SnO_2$:Ag/Ag nanoparticles hybrid films were synthesized on quartz substrates using the sol-gel method. Fig. 1 shows the schematic synthetization process of the $SnO_2$:Ag/Ag nanoparticles hybrid films. An undoped $SnO_2$ layer was first deposited on quartz substrates by sol-gel method. The detailed synthetization method of the undoped $SnO_2$ layer can be found in our previous work [13]. Then a layer of silver nitrate ($AgNO_3$) sol was spin-coating on the undoped $SnO_2$ layer. Finally, the films were annealed in a horizontal quartz-tube furnace exposed in the air at 500 °C for 1 h to obtain the $SnO_2$:Ag/Ag nanoparticles hybrid films. The Ag concentration in the hybrid film can be controlled by changing $AgNO_3$ concentration in the sol. Four samples with various Ag concentration were obtained and are denoted as T0, T1, T2 and T3, corresponding to Ag concentration of 0, 0.5 at.%, 1 at.% and 2 at.%, respectively.

X-ray diffraction (XRD) measurements were carried out for structural characterization using a powder diffract meter with a Cu $K\alpha$ radiation. The optical absorption measurements were performed using a UV–vis-near-IR spectrophotometer. The morphologies of the samples were characterized by using scanning electron microscope (SEM). A transmission electron microscope (TEM) was used to examine the crystalline structure of the samples. The photoluminescence (PL) measurements were performed using a He-Cd laser with a 325-nm line as the excitation source. The chemical states of Ag in the hybrid films were detected using x-ray photoelectron spectroscopy (XPS) with Al $K\alpha$ ($h\nu = 1486.6$ eV) x-ray radiation source.

First-principles calculations were performed using the VASP code with the projector augmented wave (PAW) method within the frame of density function theory (DFT) [28–31]. All calculations were carried out using the hybrid functional as proposed by Heyd, Scuseria, and Ernzerhof (HSE) [32,33]. The *d* electrons of Sn and Ag atoms were treated as valence electrons. A 72-atom $2 \times 2 \times 3$ $SnO_2$ supercell with the rutile structure was constructed. To simulate Ag doping in $SnO_2$, a Sn atom is replaced by an Ag atom in the supercell. The cutoff energy for the plane-wave basis set is 400 eV. In the calculations, all the atoms are allowed to relax until the Hellmann–Feynman forces acting on them become less than 0.01 eV/Å. Although the calculated bandgap of pure $SnO_2$ is underestimated within HSE framework (2.77 eV), i.e. smaller than the experimental value [12], it does not affect our discussion on the results.

## 3. Results and discussion

Fig. 2a shows the XRD patterns of all samples grown on quartz substrates. It is found that all the thin films are polycrystalline with rutile structure. For the $SnO_2$:Ag film with 0.5 at.% Ag concentration (sample T1), no diffraction peak of metal Ag or Ag related phase is observed, indicating that the Ag atoms are doped into $SnO_2$. As increasing Ag concentration (>0.5 at.%, T2 and T3), the diffraction peaks of metallic Ag are observed, implying existence of metal Ag phase in the films. In order to further check the existence of metal Ag in the $SnO_2$ films, XPS measurements were carried out. Fig. 2b shows the Ag 3d XPS spectra of the 2.0 at.% Ag-doped $SnO_2$ film (T3) before and after its surface was etched by Ar ion. Before etching, there is a strong peak and a weak shoulder for both Ag $3d_{5/2}$ and $3d_{3/2}$, respectively. The strong peak is attributed to $Ag^+$ and the weak shoulder to $Ag^0$ [34,35]. The fitting peaks are located at 367.9, 368.8, 373.9 and 374.8 eV, which is corresponding to $Ag^+$ $3d_{5/2}$, $Ag^0$ $3d_{5/2}$, $Ag^+$ $3d_{3/2}$ and $Ag^0$ $3d_{3/2}$, respectively. After etching, the intensity of the shoulder is significantly decreases, indicating that metal Ag composition is reduced. The XPS results suggest that the $Ag^+$ ions, as acceptor dopants, are derived from the Sn sites in $SnO_2$ and the metal $Ag^0$ mainly exists on the surface of the $SnO_2$ films. Fig. 2c shows the SEM image of the 2.0 at.% Ag-doped $SnO_2$ thin films. It is observed that the ball-shaped Ag particles are scattered on the surface of $SnO_2$ thin films. The grain sizes of Ag particles are in the range of 300–500 nm, indicating that the size of Ag particles is in nanoscales. A cross-sectional TEM image of the Ag-doped $SnO_2$ thin films with Ag concentration of 2 at.% is shown in Fig. 2d. A sharp interface between the crystalline film and amorphous substrate is observed.

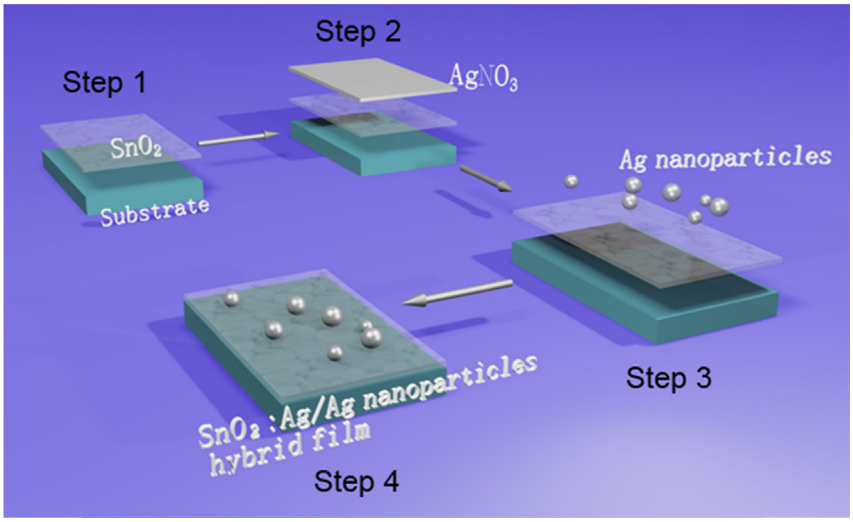


**Fig. 1.** Schematic fabrication process of the Ag-doped $SnO_2$ hybrid thin films with Ag nanoparticles surface modification.

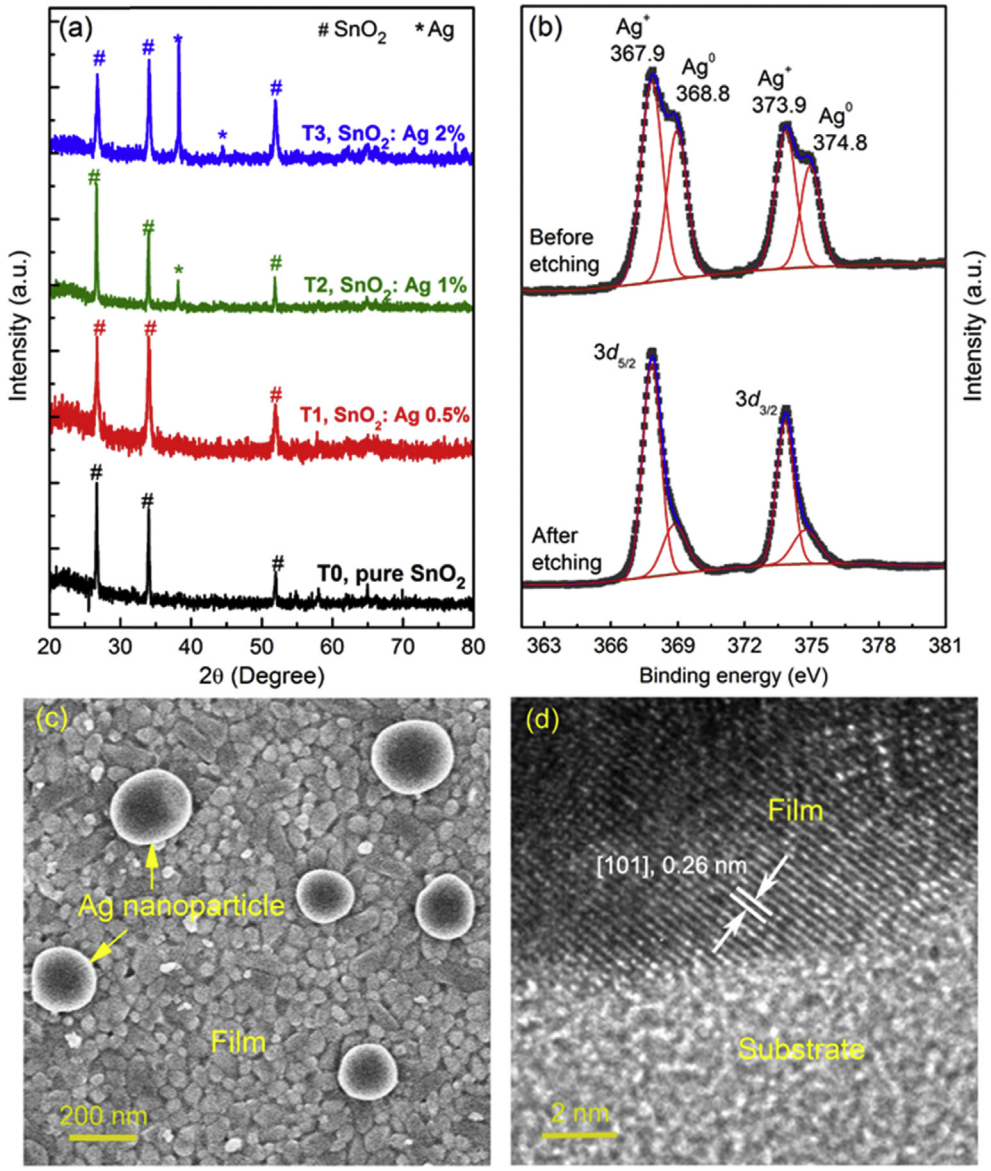


**Fig. 2.** Structural, chemical state and surface morphological characterizations of the $SnO_2$:Ag/Ag nanoparticles hybrid thin films. (a) XRD patterns of the undoped and Ag-doped $SnO_2$ films with various Ag concentration grown on quartz substrates. (b) Ag 3d XPS spectra of the Ag-doped $SnO_2$ films with Ag concentration of 2 at.% (sample T3). (c) Surface SEM image of the Ag-doped $SnO_2$ thin films with Ag concentration of 2 at.%. (d) Cross-sectional TEM image of the Ag-doped $SnO_2$ thin films with Ag concentration of 2 at.%.

To examine the effect of Ag doping and Ag nanoparticle on PL properties of $SnO_2$ films, we performed room temperature PL spectra for all samples grown on quartz substrates, as shown in Fig. 3a. For the undoped $SnO_2$ (T0), only one visible light emission band centered at ~ 540 nm was observed, which is attributed to the defect states related to the presence of structural defect like oxygen vacancies [36]. No NBE emission in the UV region was observed due to the dipole-forbidden rule. Compared with the undoped $SnO_2$ thin film, a dominant UV emission peak centered at 375 nm was observed for the 0.5 at.% Ag-doped $SnO_2$ film (T1), indicating that Ag doping can break the dipole-forbidden rule to realize UV light emission. Moreover, the UV emission intensity of the 1.0 at,% (T2) and 2.0 at.% (T3) Ag-doped $SnO_2$ films significantly increase. The enhancement ratio of the UV emission of the 2.0 at.% Ag-doped $SnO_2$ was almost 30-fold higher than that of the 0.5 at.% Ag-doped $SnO_2$. To see the change of PL intensity clearly, a logarithmic scale is adopted for the PL spectra, as shown in the inset of Fig. 3a. It is obviously that the UV emission enhancement is attributed to the interaction between the radiative recombination in $SnO_2$:Ag and SPs arising from Ag nanoparticles interfaces. The UV emission enhancement can be explained as follows. Electron-hole pairs are first generated in Ag-doped $SnO_2$ films by He–Cd laser. The emission energy can transfer to the SPs when the gap energy of $SnO_2$ is comparable to the electron vibration energy of SPs at the metal-Ag/$SnO_2$:Ag interface. Then the energy from metal/semiconductor SPs should be effectively transferred to the opposite air/metal surface SPs. Finally, the energy can be extracted as light by scattering of SPs at air/metal surface due to the surface roughness.

Fig. 3b shows the plot of $(\alpha h\nu)$ [2] vs. the photon energy $h\nu$ of the undoped and Ag-doped $SnO_2$ thin films. The optical bandgap of the undoped $SnO_2$ film is determined to be ~3.9 eV, in agreement with the values of 3.6–3.9 eV from the previous reports [12,13]. Meanwhile, the optical bandgap of the undoped $SnO_2$ film is much larger than the fundamental bandgap of 3.3–3.4 eV, indicating the nature of dipole-forbidden bandgap transition. As the Ag concentration

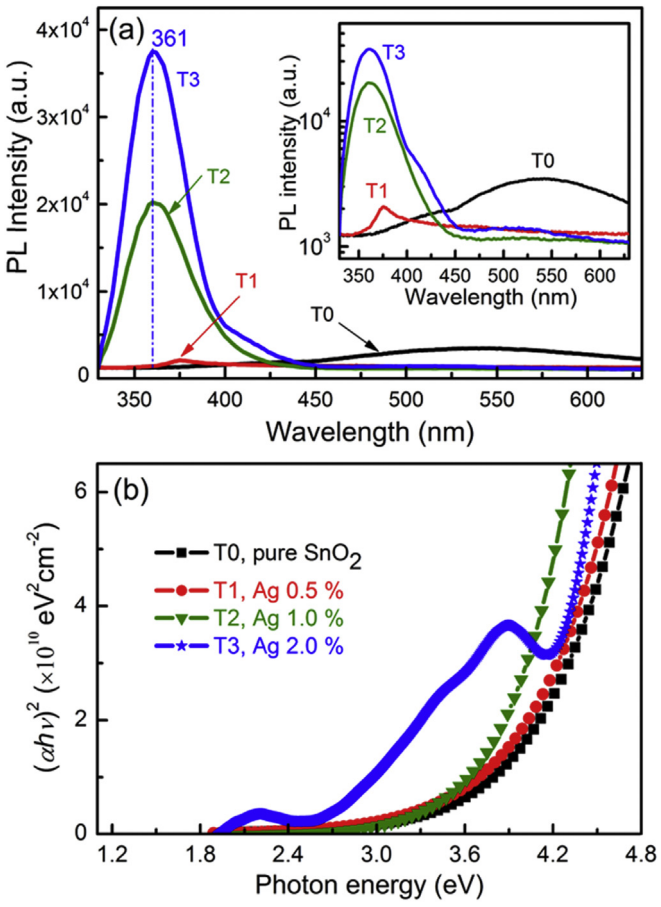


**Fig. 3.** Room temperature (a) PL and (b) optical absorption spectra of the undoped and Ag-doped $SnO_2$ thin films grown on quartz substrates. The inset in (a) shows a logarithmic scale of the PL spectra for clear demonstrating the weak emission.

increases, the optical bandgap shows a significant redshift, which is due to the acceptor states in the bandgap induced by Ag doping [37]. Therefore, the defect states relevant to Ag impurities play key role in breaking the dipole-forbidden rule. Additionally, it should be noted that a strong band-tail absorption band, smaller the optical bandgap of undoped $SnO_2$, is observed in the absorption spectra of the 2.0% at.% Ag-doped $SnO_2$ films (T3). The strong band-tail absorption is attribute to the SPR absorption of Ag nanoparticles on the film surface, which is consist with the PL result.

Finally, to better understand the recovering UV emission in Ag-doped $SnO_2$, we performed fist-principles calculations within the frame of DFT. Fig. 4a and b shows the calculated energy band structures of the perfect and Ag-doped $SnO_2$ systems, respectively. The calculated fundamental bandgap of the perfect $SnO_2$ systems are 2.77 eV. For the Ag-doped $SnO_2$ system, impurity states relevant to Ag substituting Sn is found in the gap. To better understand the transition, optical absorption spectra of the perfect and Ag-doped $SnO_2$ systems were calculated, as shown in Fig. 4c. To simulate the optical properties of the polycrystalline $SnO_2$, the polarized absorption from x-, y- and z-direction is averaged. For the perfect $SnO_2$, the onset of the optical absorption edge is much higher than the calculated fundamental bandgap of 2.77 eV, indicating that the band edge transition is forbidden in perfect $SnO_2$. For the Ag-doped $SnO_2$, the optical absorption edge significantly moves towards to low energy side and there exists a strong band-tail absorption near fundamental bandgap, in consistence with the results of the optical absorption spectra. The calculated results suggest that Ag doping

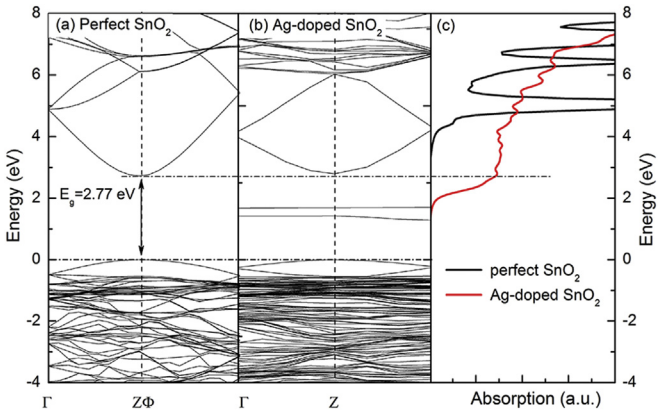


**Fig. 4.** Electronic structures of the perfect and Ag-doped $SnO_2$ from the first-principles calculations. Band structures of the (a) perfect and (b) Ag-doped $SnO_2$. (c) Polycrystalline optical absorption spectra of the perfect and Ag-doped $SnO_2$.

can break dipole-forbidden rule of $SnO_2$, well supporting our experimental results.

## 4. Conclusion

In summary, dipole-forbidden rule of $SnO_2$ can be broken via Ag doping and UV NBE emission also can be recovered via Ag doping. A giant enhancement of recovered UV emission in $SnO_2$:Ag/Ag nanoparticles hybrid film is observed, which is derived from SPs-mediated emission enhancement. Our findings may pave the way for the further development of high-efficiency $SnO_2$-based UV light-emitting diodes and laser diodes.

## Acknowledgements

This work was supported by the National Natural Science Foundation of China under Grant Nos. 10874178, 11074093, 61205038, 11464035 and 11274135, Natural Science Foundation of Jilin Province under Grant Nos. 201115013, 20140101052JC, The Science and Technology Development Project of Jilin Province under grant No. 20170101142JC. This work was supported by High Performance Computing Center of Jilin University, China.

## References

[1] Y. Li, R. Deng, W. Lin, Y. Tian, H. Peng, J. Yi, B. Yao, T. Wu, Phys. Rev. B 87 (15) (2013) 155151.
[2] G.Z. Xing, Y. Wang, J.I. Wong, Y.M. Shi, Z.X. Huang, S. Li, H.Y. Yang, Appl. Phys. Lett. 105 (14) (2014) 143905.
[3] G.Z. Xing, J.B. Yi, F. Yan, T. Wu, S. Li, Appl. Phys. Lett. 104 (20) (2014) 202411.
[4] Y. Li, R. Deng, B. Yao, G. Xing, D. Wang, T. Wu, Appl. Phys. Lett. 97 (10) (2010) 102506.
[5] J.J. Lee, G.Z. Xing, J.B. Yi, T. Chen, M. Ionescu, S. Li, Appl. Phys. Lett. 104 (1) (2014) 012405.
[6] K.X. Jin, Y.F. Li, Z.L. Wang, H.Y. Peng, W.N. Lin, A.K.K. Kyaw, Y.L. Jin, K.J. Jin, X.W. Sun, C. Soci, T. Wu, AIP Adv. 2 (4) (2012) 042131.
[7] B. Zhang, B. Yao, S. Wang, Y. Li, C. Shan, J. Zhang, B. Li, Z. Zhang, D. Shen, J. Alloys Compd. 503 (1) (2010) 155–158.
[8] W.W. Liu, B. Yao, B.H. Li, Y.F. Li, J. Zheng, Z.Z. Zhang, C.X. Shan, J.Y. Zhang, D.Z. Shen, X.W. Fan, Solid State Sci. 12 (9) (2010) 1567–1569.
[9] W. Liu, B. Yao, Y. Li, B. Li, C. Zheng, B. Zhang, C. Shan, Z. Zhang, J. Zhang, D. Shen, Appl. Surf. Sci. 255 (13–14) (2009) 6745–6749.
[10] Y. Li, B. Yao, R. Deng, B. Li, Z. Zhang, C. Shan, D. Zhao, D. Shen, J. Alloys Compd. 575 (2013) 233–238.
[11] Y. Huang, Y. Li, B. Yao, Z. Ding, R. Deng, L. Zhang, H. Zhao, J. Phys. D. Appl. Phys. 48 (46) (2015) 465103.
[12] Y. Li, W. Yin, R. Deng, R. Chen, J. Chen, Q. Yan, B. Yao, H. Sun, S.-H. Wei, T. Wu, NPG Asia Mater. 4 (11) (2012) e30.
[13] H. Zhou, R. Deng, Y.-F. Li, B. Yao, Z.-H. Ding, Q.-X. Wang, Y. Han, T. Wu, L. Liu, J. Phys. Chem. C 118 (12) (2014) 6365–6371.
[14] R. Chen, G.Z. Xing, J. Gao, Z. Zhang, T. Wu, H.D. Sun, Appl. Phys. Lett. 95 (6)

(2009) 061908.
[15] M. Batzill, U. Diebold, Prog. Surf. Sci. 79 (2–4) (2005) 47–154.
[16] K. Vinodgopal, I. Bedja, P.V. Kamat, Chem. Mater. 8 (8) (1996) 2180–2187.
[17] P.G. Harrison, M.J. Willett, Nature 332 (6162) (1988) 337–339.
[18] A. Kowal, M. Li, M. Shao, K. Sasaki, M.B. Vukmirovic, J. Zhang, N.S. Marinkovic, P. Liu, A.I. Frenkel, R.R. Adzic, Nat. Mater. 8 (4) (2009) 325–330.
[19] D. Fröhlich, R. Kenklies, R. Helbig, Phys. Rev. Lett. 41 (25) (1978) 1750–1751.
[20] K.W. Liu, Y.D. Tang, C.X. Cong, T.C. Sum, A.C.H. Huan, Z.X. Shen, L. Wang, F.Y. Jiang, X.W. Sun, H.D. Sun, Appl. Phys. Lett. 94 (15) (2009) 151102.
[21] K. Okamoto, I. Niki, A. Shvartser, Y. Narukawa, T. Mukai, A. Scherer, Nat. Mater. 3 (9) (2004) 601–605.
[22] K. Okamoto, I. Niki, A. Scherer, Y. Narukawa, T. Mukai, Y. Kawakami, Appl. Phys. Lett. 87 (7) (2005) 071102.
[23] P. Cheng, D. Li, Z. Yuan, P. Chen, D. Yang, Appl. Phys. Lett. 92 (4) (2008) 041119.
[24] I. Gontijo, M. Boroditsky, E. Yablonovitch, S. Keller, U.K. Mishra, S.P. DenBaars, Phys. Rev. B 60 (16) (1999) 11564–11567.
[25] A. Liebsch, Phys. Rev. Lett. 71 (1) (1993) 145–148.
[26] H. Ehrenreich, H. Philipp, Phys. Rev. 128 (4) (1962) 1622–1629.
[27] J. Lu, J. Li, C. Xu, Y. Li, J. Dai, Y. Wang, Y. Lin, S. Wang, ACS Appl. Mater. Interfaces 6 (20) (2014) 18301–18305.
[28] P.E. Blöchl, Phys. Rev. B 50 (24) (1994) 17953–17979.
[29] G. Kresse, D. Joubert, Phys. Rev. B 59 (3) (1999) 1758–1775.
[30] G. Kresse, J. Furthmüller, Phys. Rev. B 54 (16) (1996) 11169–11186.
[31] G. Kresse, J. Furthmüller, Comput. Mater. Sci. 6 (1) (1996) 15–50.
[32] J. Heyd, G.E. Scuseria, M. Ernzerhof, J. Chem. Phys. 118 (18) (2003) 8207–8215.
[33] J. Heyd, G.E. Scuseria, M. Ernzerhof, J. Chem. Phys. 124 (21) (2006) 219906.
[34] T.N. Xu, X. Li, Z. Lu, Y.Y. Chen, C.H. Sui, H.Z. Wu, Appl. Surf. Sci. 316 (0) (2014) 62–65.
[35] R. Deng, B. Yao, Y.F. Li, T. Yang, B.H. Li, Z.Z. Zhang, C.X. Shan, J.Y. Zhang, D.Z. Shen, J. Cryst. Growth 312 (11) (2010) 1813–1816.
[36] S.U. Lee, B. Hong, W.S. Choi, J. Vac. Sci. Technol. A 27 (4) (2009) 996–1000.
[37] W. Li, S.-h. Wei, X. Duan, Phys. Lett. A 378 (30–31) (2014) 2275–2279.